An Advanced Algorithm for Accurate Retrieval of Liquid Water Cloud Properties Using Spaceborne Radar

Jiajing Du, Jinming Ge, Jianping Huang, Yize Li, Chi Zhang, Xiaoyu Hu, Bochun Liu, Xiaojie Li, Yucheng Qiu, and Yuhang Zhu

***Abstract*—Low cloud microphysical properties, including liquid water content (LWC), cloud effective radius (CER), and cloud optical thickness (COT), are fundamental to climate modeling and weather prediction. However, existing remote sensing techniques often rely on a priori data and passive instrument observations, which limit the accuracy and consistency of retrievals, particularly in complex cloud regimes. In this study, we present an innovative radar-based algorithm that retrieves LWC, CER, and COT directly from CloudSat millimeter-wavelength cloud profiling radar (CPR) observations. Unlike conventional approaches, our method derives physically consistent cloud properties with minimal reliance on ancillary data, thereby overcoming the inherent limitations of current algorithms. We demonstrate the efficacy of this method through detailed comparisons with established cloud products from CloudSat, MODIS, and AMSR2 sensors. The results show improved accuracy in LWC retrievals and a more consistent vertical distribution of CER and COT, particularly in challenging low marine boundary layer clouds. This novel algorithm offers a significant advancement in cloud remote sensing, facilitating more reliable cloud property retrievals for enhanced climate model simulations. The method is fully applicable for CloudSat's 18-year record and the latest space radar mission of EarthCare, offering an essential tool to better capture the vertical complexity of clouds and to advance global cloud data quality for climate research.**

***Index Terms*—Cloud radar, low clouds, mass absorption attenuation, microphysical properties.**

I. Introduction

LOW-LEVEL clouds (LLCs), forming around 2–3-km altitude, are predominantly composed of liquid water droplets and are extensively distributed across the Earth's surface. Due to their abundance of small droplets, LLCs are highly effective at reflecting incoming solar radiation and influencing precipitation patterns. Consequently, they play a critical role in regulating the planet's radiation budget and hydrological cycle [1]. The microphysical properties of LLC, including liquid water content (LWC), cloud effective radius (CER), and cloud optical thickness (COT), are pivotal in governing their radiative and precipitation processes. For instance, higher LWC and larger droplets enhance precipitation potential, while smaller CER leads to more reflective clouds that may suppress rainfall [2], [3], [4]. As climate changes, variations in these microphysical properties may induce feedbacks that either amplify or mitigate warming through further interactions with solar and terrestrial radiation. However, accurately representing LLC properties in models remains one of the largest sources of uncertainty, contributing significantly to the spread in climate sensitivity estimates [5], [6], [7], [8]. Enhanced observations are essential to address these uncertainties by enabling better assessments and constraints on cloud characteristics, thereby advancing our understanding of cloud microphysics and improving their representation in numerical models.

Currently, a variety of passive and active remote sensing instruments provide comprehensive data on cloud physical properties [9]. Passive sensors, such as visible and infrared imagers, or microwave radiometers [10], [11], [12], measure reflectance or emittance in channels sensitive to cloud features, offering broad spatial coverage with high temporal frequency. However, they struggle to capture the vertical structure of clouds, as their signals primarily originate from the cloud layer closer to the instruments. This limitation introduces significant errors, particularly when detecting multilayer or optically thick clouds. In contrast, active sensors like lidar and radar emit electromagnetic waves and measure backscattered signals, enabling them to retrieve high-resolution vertical profiles of cloud layers. Nevertheless, their performance can be compromised by signal attenuation within the cloud layer and environmental interferences, which may also affect the detection accuracy active instrument [13], [14], [15], [16]. Sensors onboard satellite are particularly effective in obtaining global cloud physical properties [17], [18]. Especially the W-band (94 GHz) cloud profiling radar (CPR) on CloudSat, which is highly sensitive to small cloud droplets and ice crystals, has made significant advancements in cloud physics and dynamics by providing unprecedented vertical cloud pro-

Received 5 March 2025; revised 9 September 2025 and 7 November 2025; accepted 29 November 2025. Date of publication 5 December 2025; date of current version 18 December 2025. This work was supported by the National Natural Science Foundation of China under Grant 42275076 and Grant 42427804, in part by the Youth Special Funds for the Heavy Rain and Drought-Flood Disasters in Plateau and Basin Key Laboratory of Sichuan Province under Grant SCQXKJQN202508, and in part by the Fundamental and Interdisciplinary Disciplines Breakthrough Plan of the Ministry of Education of China under Grant JYB2025XDXM910. *(Corresponding author: Jinming Ge.)*

Jiajing Du is with the Key Laboratory for Semi-Arid Climate Change of the Ministry of Education and College of Atmospheric Sciences, Lanzhou University, Lanzhou 730000, China, and also with the Institute of Plateau Meteorology, China Meteorological Administration, Chengdu 610213, China.

Jinming Ge, Jianping Huang, Yize Li, Chi Zhang, Bochun Liu, Xiaojie Li, Yucheng Qiu, and Yuhang Zhu are with the Key Laboratory for Semi-Arid Climate Change of the Ministry of Education and the College of Atmospheric Sciences, Lanzhou University, Lanzhou 730000, China (e-mail: gejm@lzu.edu.cn).

Xiaoyu Hu is with Chongqing Research Institute of Big Data, Chongqing 400041, China, and also with the School of Mathematical Sciences, Peking University, Beijing 100871, China.

Digital Object Identifier 10.1109/TGRS.2025.3640651

files on a global scale [19], [20], [21], [22], [23]. Although CloudSat operations ceased at the end of 2023, the extensive data collected over its 18-year mission remain invaluable for cloud physics investigations and for integrating active and passive observations using machine learning methods.

Despite these advancements, discrepancies persist between cloud properties retrieved using different techniques due to their reliance on varying physical principles. For instance, the current CPR algorithm derives cloud properties from forward modeling by assuming a lognormal distribution for cloud droplet size [24], [25], [26]. However, this assumption does not always reflect the true variability of the particle size distribution within the cloud, inducing potential inaccuracies in retrievals. Larger particles can bias radar measurements, skewing the CER estimates, while signal attenuation of the radar further exacerbates retrieval uncertainties. Integration of radar data with visible optical depth from MODIS has improved the accuracy of cloud products like the radar–visible optical depth (RVOD) Cloud Water Content (2B-CWC-RVOD, hereafter RVOD) [25]. However, the RVOD's dependency on MODIS data limits its temporal and spatial availability, particularly since CloudSat deviated from the A-Train constellation in 2018, preventing synchronization with MODIS observations.

Comparisons with aircraft in situ samplings, other satellite-based passive remote sensing instruments and ground-based cloud radar observations reveal that the difference between various cloud products can be more than 100% with CloudSat products showing significant bias [27], [28], [29], [30], especially in the presence of large particles associated with high reflectivity [31], [32]. These differences present challenges for accurately capturing cloud 3-D structures, calculating radiative flux, and developing consistent parameterizations to improve understanding of cloud-radiation interactions and their climate implications. Therefore, developing novel retrieval algorithms that address these limitations remains critical for maximizing the utility of CloudSat data for improving cloud characteristic retrieval and reducing uncertainties in climate projections.

The Southern Ocean (SO), one of the most remote and cloud-dominated regions on Earth, presents significant challenges due to persistent biases in the representation of LLCs and their radiative effects in climate models. These biases contribute to considerable uncertainties in global climate predictions, underscoring the critical need for improved observational data and retrieval methods [9], [33], [34], [35], [36]. In this study, we enhanced our previously developed self-consistent mass absorption algorithm, originally designed for ground-based Ka-band cloud radar, to adapt it for CloudSat observations. This goal is to generate high-quality retrievals of cloud microphysical properties over the SO area.

By constructing a radar detection principles-based scheme in the Rayleigh scattering regime, our approach eliminates the need to assume a specific droplet size distribution and ensures the retrievals are free of reliance on other passive instruments. We retrieve LWC, CER, and COT by leveraging the intrinsic relationships among these variables. Section III of this article details the development and application of the retrieval method. Section IV provides a comprehensive evaluation of the algorithm, including comparisons with CloudSat official products and other passive satellite-derived datasets, where the details of the instruments used in this study are introduced in Section II. Finally, Section V summarizes the main findings, discusses the implications for climate research, and highlights the improvement of this method for the consistency and accuracy of LLC property retrievals.

II. Instrument and Dataset

CloudSat is a key component of the National Aeronautics and Space Administration (NASA)'s A-Train satellite constellation, launched in 2006, and is equipped with the CPR operating at a frequency of 94 GHz (W-band). The CPR receives signals backscattered by hydrometeors with cross-track resolution of 1.4 km and along-track resolution of 1.7 km, and a vertical resolution of 0.24 km. Each profile consists of 125 samples, and the minimum detectable reflectivity factor is approximately −30 dBZ, providing high-resolution profiles of cloud properties. CloudSat offers a variety of cloud features in different data products. The 2B-GEOPROF product identifies cloud echoes as "cloud mask." The 2B-CLDCLASS-LIDAR product, which combines radar and lidar data, provides detailed information about cloud boundaries (e.g., cloud base and top), and classifies clouds by phase (e.g., liquid, ice, and mixed phase) [37]. In addition, CloudSat offers comprehensive cloud microphysical properties through its Radar-Only (RO) and RVOD cloud water content products. These products allow for the retrieval of key cloud characteristics, such as LWC, LWP, and CER. The CER can be converted from the geometric mean radius r_g provided by RVOD product utilizing the interconnection between physical variables under the assumption that the DSD satisfies a lognormal distribution with the geometric standard deviation $\sigma_{\log}$ is fixed at 0.38 [26].

The MODIS and AMSR2 onboard the Aqua and Global Change Observation Mission 1st-Water (GCOM-W1) satellite, operating in the A-Train satellite, capture solar reflectance in 36 spectral channels ranging from visible to the infrared wavelengths (0.4–14.4 μm), and 16 channels with seven frequencies varying from 6.9 to 89 GHz, respectively [38], [39]. MODIS channels at 1.6, 2.1, and 3.7 μm, along with the AMSR2 channel near 23 GHz, are sensitive to water vapor, enabling the retrieval of key cloud properties such as LWP, COT, and CER [32], [40], [41]. Notably, while MODIS is limited to solar radiation, the MWR in the microwave channels provides continuous cloud observations throughout the day with uncertainty in LWP retrievals typically within about 5–8 g·m^{-2} [42].

In this study, since the most recent comprehensive data products prior to the CloudSat's orbit change are from 2017, and our method relies solely on radar wavelength and cloud droplet phase, both independent of temporal and spatial variations, we selected one-year of CloudSat CPR observations over the SO region (40°S~65°S) [33], [34] in 2017 to retrieve cloud microphysical properties. The feasibility of applying spaceborne radar-based cloud property retrievals is assessed by comparing with corresponding cloud products from MODIS-1KM-AUX and AMSR2-AUX. These products, produced by

CloudSat Data Processing Center (DPC), are collocated with CPR in spatial and temporal with CPR footprint, ensuring consistent resolution and effective comparison between cloud products from different instruments.

III. Retrieval Method

In this study, we propose a novel method for retrieving cloud microphysical properties that significantly improves the accuracy and consistency of LWC, CRE, and COT, addressing limitations of previous empirical-based methods. Prior approaches often relied on simplified empirical formulas that assumed specific DSDs, resulting in large uncertainties in the retrievals of these cloud properties. In contrast, our method avoids the assumptions and instead incorporates the intrinsic relationship between radar reflectivity and cloud droplet size while accounting for the attenuation of radar signals due to LWC mass absorption.

According to the radar detection principle, the intrinsic radar reflectivity factor Z_e is proportional to the sixth power of the cloud droplet radius that characterizes the particles' backscattering intensity of the radar power, while the radar-measured reflectivity Z_m is obtained after the radar power attenuated by cloud water content. This attenuation is incorporated into our model through a physical relationship expressed as follows:

$$Z_e(h_i) = Z_m(h_i)\, e^{0.46 \int_{h_t}^{h_i} k(s) ds} \tag{1}$$

where radar reflectivity $Z_e(h_i)$ at a given height is corrected from attenuation based on cloud LWC, and k is the one-way attenuation coefficient in units of dB/km. The attenuation is contributed to by both gas (i.e., oxygen and water vapor) and cloud droplet absorption. Considering that the attenuation of gas can be neglected compared to cloud droplets and the attenuation caused by cloud droplets satisfies the Rayleigh approximation, the attenuation caused by cloud droplet absorption is only considered in this study (i.e., $k = k_c$) and k_c is proportional to the cloud LWC, that is $k_c = 0.4343(6\pi)/(\lambda\rho_0) Im(-(m^2-1)/(m^2+2))\text{LWC} = K^*\text{LWC}$, where ρ_0 is the density of water with the value of 1 g/m^3. The K^* in units of (dB/km)/(g/m^3) is determined by the radar wavelength and the imaginary part of the refractive index, depending on the temperature and phase, but independent of the cloud DSD. This correction ensures that the retrievals are not biased by assumptions about the DSD. By converting (1) into a Bernoulli differential equation as shown in the Appendix, we derived a more accurate expression for LWC that is free from empirical coefficients and prior assumptions with reference to the LWC retrieval method applicable to ground-based radar [43]. Unlike previous studies, we modified the integration direction of the Bernoulli equation from the cloud top to the cloud base to account for the spaceborne radar's top-down detection, as shown in (2). Namely, the LWC expression in this study is gained by combining the equations calculated by integrating the Bernoulli differential equation from the cloud top to the cloud base and at a certain height within the cloud. The complete process of integration is illustrated in the Appendix

$$\text{LWC}(h_i) = \frac{Z_m^b(h_i)\left[\exp(0.46bK^*\text{LWP}) - 1\right]}{I(h_t h_l) + \left[\exp(0.46bK^*\text{LWP}) - 1\right] I(h_i h_l)}$$

$$I(h_i, h_l) = \int_{h_i}^{h_l} 0.46bK^* Z_m^b(s)\, ds \tag{2}$$

where h_l and h_t indicate the radar gate at the cloud base and top, respectively. The optimal parameters (i.e., b and LWP) in (2) can be obtained by minimizing the error between the reconstructed and measured reflectivity through applying the trust region reflective (TRR) method.

Given that the CER is defined as the ratio of the third to the second moment of DSD and that the LWC and Z are proportional to the third and sixth moment of DSD, respectively, we construct a retrieval expression for CER based on these fundamental physical relationships under the assumption of lognormal cloud DSD [44] as shown by

$$\text{CER}(h_i) = r_m^{\frac{4}{9}} \left[\frac{\pi\rho_w}{48} \frac{Z_e(h_i)}{\text{LWC}(h_i)}\right]^{\frac{5}{27}} \tag{3}$$

where the parameter r_m is the median radius with optimal constant value of 13.1 μm selected by performing sensitivity analysis on different parameters (i.e., r_m and logarithmic spectral width σ_x) [44] under the premise that the cloud DSD satisfies a lognormal distribution, and the uncertainty of retrieval results caused by the parameter r_m variation is only 11% [44]. In addition, COT is the integral of the extinction caused by the cloud droplets, and can be expressed as a function of LWC and CER [44]

$$\text{COT} = \int_{h_t}^{h_l} \text{COT}(h)\, dh = \int_{h_t}^{h_l} \frac{3}{2} \frac{\text{LWC}(h)}{\text{CER}(h)} dh. \tag{4}$$

This approach lies in its ability to derive essential cloud properties without relying on empirical coefficients or passive instruments. By integrating the physical and mathematical definitions of multiple cloud microphysical parameters into the radar equation, we construct an interactive and coordinated adaptive inversion scheme that considers both particle backscattering and cloud water mass absorption during radar wave transmission. This scheme ensures that the retrieval of cloud properties is dynamically linked to the variations of cloud physical features, and can not only improve the accuracy of microphysical property retrievals, but also reduce uncertainty by minimizing reliance on preassumed particle distributions. Ultimately, this method provides a more robust and physically grounded framework for cloud property retrieval from spaceborne radar observations, making it a significant advancement over traditional techniques.

IV. Results and Discussion

The process begins with the identification of cloud boundaries, which are determined by combining cloud base and top heights [indicated by black and purple dots in Fig. 1(a)] with a cloud mask value greater than 20 [see Fig. 1(b)]. This is followed by the selection of liquid water clouds based on cloud phase classification from the 2B-CLDCLASS-LIDAR product as displayed in Fig. 1(c). Once the cloud boundaries are defined, the cloud microphysical properties, such as LWC, CER, and COT, are retrieved by applying the radar-measured reflectivity factor of liquid water clouds within the identified boundaries, as shown in Fig. 1(d)–(f), respectively.

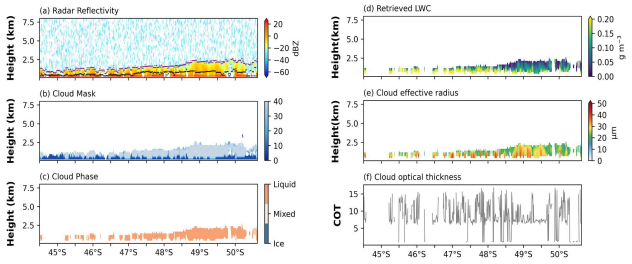

Fig. 1. Case of a single-layer cloud over the SO region. (a) Latitude–height profiles of the reflectivity and the best estimated cloud base and top marked by the black and purple dots, respectively; Time–height profiles of (b) cloud mask, (c) cloud phase, (d) retrieved LWC, (e) retrieved CER, and (f) retrieved COT represented by gray solid line.

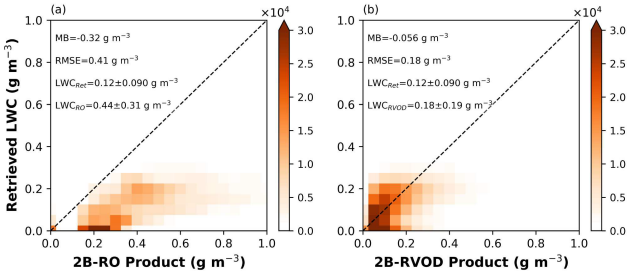

Fig. 2. Comparison of the retrieved LWC with (a) RO and (b) RVOD product provided by CloudSat. The "MB" and "RMSE" in the text box at the upper left corner of each subgraph represent the MB and the RMSE between the retrieved results and the CloudSat product.

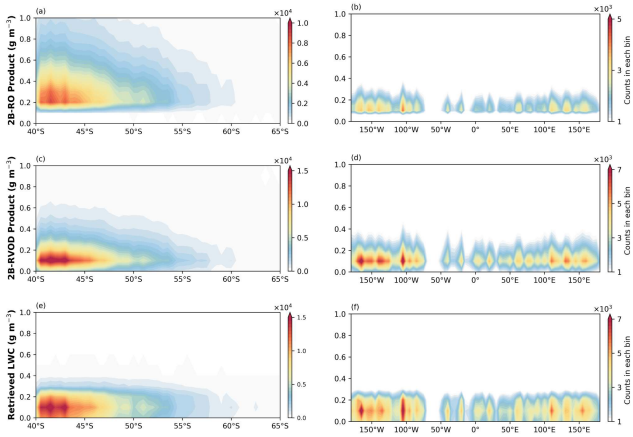

Fig. 3. Distribution of cloud LWC provided by (a) and (b) RO, (c) and (d) RVOD, and (e) and (f) our method with latitude (left column) and longitude (left column), respectively.

The results show that the retrieved LWC values are generally below 0.2 g/m^3, with peak LWC concentrations near the cloud base. This is accompanied by large cloud particles, indicated by CER values exceeding 20 μm, reflecting the presence of larger droplets at lower altitudes. These findings align with the known behavior of LWC, which typically decreases with altitude as larger precipitation particles fall toward the surface. This validates our method's ability to accurately capture the vertical distribution of cloud properties and supports its use in cloud microphysics retrievals from spaceborne radar data [45].

A. Comparison and Evaluation of LWC Retrieval Accuracy

The comparison between the LWC retrieved by our method (denoted as $\mathrm{LWC_{Ret}}$, hereafter) and the LWC provided by RO

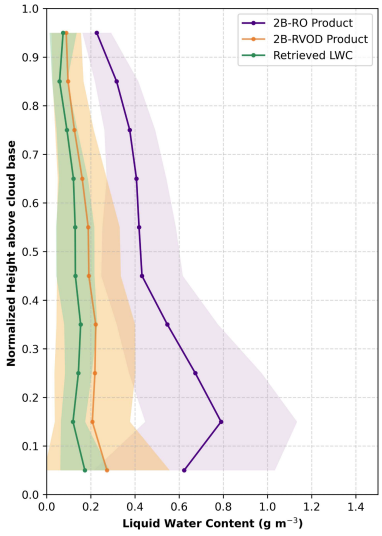

Fig. 4. Profiles of LWC retrieved by our method (green solid line), 2B-RO product (purple solid line), and 2B-RVOD product (orange solid line). The solid dots and shaded region are the mean and standard deviation of LWC within each normalized height bin of 0.1, where the normalized height is the ratio of the distance from the cloud base at any height within the cloud to the cloud thickness.

(hereafter $\mathrm{LWC_{RO}}$) and the RVOD (hereafter $\mathrm{LWC_{RVOD}}$) product are shown in Fig. 2(a) and (b). The retrieval uncertainties are quantified using the mean bias (MB) and root mean square error (RMSE) between our retrieval results and the CloudSat products. The results reveal that $\mathrm{LWC_{Ret}}$ (0.12 ± 0.09 g·m^{-3}) exhibits smaller MB (-0.056 versus -0.32 g·m^{-3}) and RMSE (0.18 versus 0.41 g·m^{-3}) compared to $\mathrm{LWC_{RO}}$, and is more consistent with $\mathrm{LWC_{RVOD}}$. In addition, the data point for $\mathrm{LWC_{Ret}}$ are more concentrated near the diagonal (i.e., the dotted line in the figure), indicating that the retrieved LWC values with uncertainty of 0.18 g·m^{-3} are closer to those from the CloudSat RVOD products. The spatial distribution of LWC obtained via different methods, respectively. As depicted in Fig. 3, the $\mathrm{LWC_{RO}}$, $\mathrm{LWC_{RVOD}}$ and $\mathrm{LWC_{Ret}}$ are predominantly concentrated between 40°S to 45°S, and the variations in $\mathrm{LWC_{Ret}}$ and $\mathrm{LWC_{RVOD}}$ with longitude shows a high frequency occurrence around 110°W and 160°W, which aligns with previous findings by Lin et al. [35], who observed higher cloud water content near 40°S and 160°W. The LWC distribution from $\mathrm{LWC_{Ret}}$ closely resembles that of $\mathrm{LWC_{RVOD}}$, but with a smaller range. Moreover, the cloud LWC from all the different approaches consistently decreases with normalized altitude within the cloud layer, as shown in Fig. 4. Notably, the $\mathrm{LWC_{Ret}}$ not only follows the same trend as $\mathrm{LWC_{RVOD}}$, but also shows a narrower distribution compared with both $\mathrm{LWC_{RVOD}}$ and $\mathrm{LWC_{RO}}$ within each altitude range. This suggests that $\mathrm{LWC_{Ret}}$ with its smaller standard deviation, provides a more uniform estimate of LWC at different heights within the cloud layer, further confirming the robustness and precision of our retrieval method.

The high-quality LWP derived from passive remote sensing instruments of AMSR2 and MODIS is compared with the results retrieved from our method, as well as the official products from CloudSat, shown in Fig. 5. A total of 20 077 profiles, where both active and passive instruments

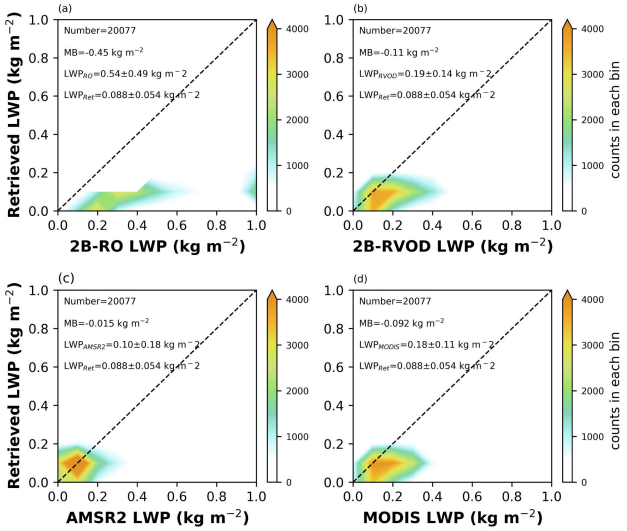

Fig. 5. Comparison of the retrieved LWP with (a) RO and (b) RVOD product provided by CloudSat and the LWP provided by (c) AMSR2 and (d) MODIS. The "MB" and "RMSE" in the text box at the upper left corner of each subgraph represent the MB and the RMSE between the retrieved results and the product.

(i.e., CloudSat, AMSR2, and MODIS) were simultaneously valid during the selected period, were analyzed for statistical evaluation. The retrieved LWP (denoted as $\mathrm{LWP_{Ret}}$), with a mean value of 0.088 kg·m^2, closely matches the LWP from the RVOD product (hereafter $\mathrm{LWP_{RVOD}}$) and shows greater consistency with AMSR2 (hereafter $\mathrm{LWP_{AMSR}}$) compared with other products (i.e., $\mathrm{LWP_{RO}}$, $\mathrm{LWP_{MODIS}}$). Specifically, the values are as follows: $\mathrm{LWP_{Ret}}$ = 0.088 kg·m^{-2}, $\mathrm{LWP_{RVOD}}$ = 0.19 kg·m^{-2}, $\mathrm{LWP_{RO}}$ = 0.54 kg·m^{-2}, $\mathrm{LWP_{AMSR}}$ = 0.10 kg·m^{-2}, and $\mathrm{LWP_{MODIS}}$ = 0.18 kg·m^{-2}. These results demonstrate that $\mathrm{LWP_{Ret}}$ aligns more closely with the microwave radiometer-derived LWP, especially compared with the overestimation of $\mathrm{LWP_{MODIS}}$, which is often influenced by the solar zenith angle (Greenwald, 2009). Furthermore, the MB between $\mathrm{LWP_{Ret}}$ and $\mathrm{LWP_{MODIS}}$ (−0.09 kg·m^2) is comparable to the MB between $\mathrm{LWP_{RVOD}}$ and $\mathrm{LWP_{MODIS}}$ (−0.11 kg·m^{-2}), which results from the fusion of MODIS and CPR data. This confirms that our algorithm can accurately provide an independent retrieval of LWP with uncertainty of 0.19 kg·m^{-2}, free from reliance on passive instruments like MODIS, addressing the limitations of existing methods that depend on such data sources.

B. Comparison and Evaluation of CER and COT Accuracy

Given that passive remote sensing instruments like MODIS provide high-quality CER primarily at the cloud top, we compare the CER retrieved using our proposed method in the cloud top layer (hereafter $\mathrm{CER^{\mathit{T}}_{Ret}}$) with those from the CloudSat RO product (hereafter $\mathrm{CER^{\mathit{T}}_{RO}}$) and the RVOD product (hereafter $\mathrm{CER^{\mathit{T}}_{RVOD}}$) at the cloud top bin. As shown in Fig. 6(a)–(c), in contrast to the cloud LWC comparison, where our method yields smaller values than the RO product, $\mathrm{CER^{\mathit{T}}_{Ret}}$ is higher than $\mathrm{CER^{\mathit{T}}_{RO}}$, with an MB of 8.11 μm and RMSE of 8.69 μm. Our retrieved CER is much closer to $\mathrm{CER^{\mathit{T}}_{RVOD}}$ and $\mathrm{CER^{\mathit{T}}_{MODIS}}$, with smaller MB (RMSE) of 3.04 μm (6.22 μm) and 1.1 μm

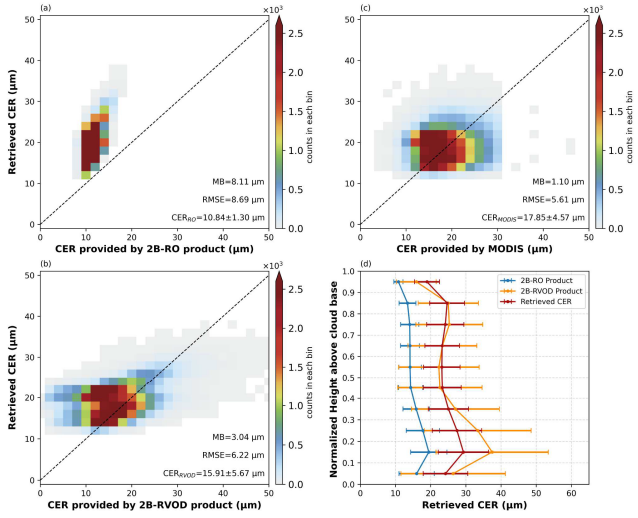

Fig. 6. Comparison of the retrieved CER at the cloud top with (a) RO, (b) MODIS, and (c) RVOD product. And (d) profiles of retrieved CER (red solid line) compared with the 2B-RO product (blue solid line) and 2B-RVOD product (orange solid line).

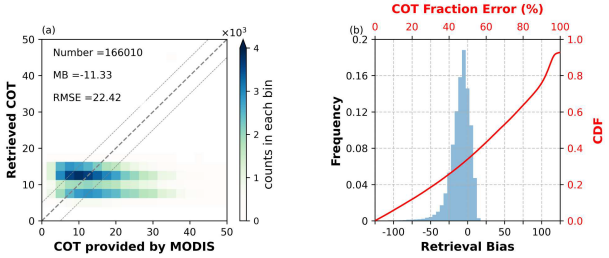

Fig. 7. (a) Comparison of the retrieved COT with the MODIS product. (b) Frequency distribution histogram of the bias between the retrieval and product (blue shading area) and the CDFs of the COT fractional error (red solid line).

(5.61 μm), respectively. These results suggest that our retrieval method improves upon the RO product and closely aligns with existing passive instruments.

Furthermore, the vertical profiles of CER, shown in Fig. 6(d), compare the retrievals from our method (hereafter $\mathrm{CER_{Ret}}$), provided by RO (hereafter $\mathrm{CER_{RO}}$) and RVOD (hereafter $\mathrm{CER_{RVOD}}$) products across each radar range gate. The CERs from all three approaches exhibit a tendency to increase and then decrease with height in the cloud layer, which can be attributed to the aggregation of particles near the cloud base as precipitation occurs below the cloud. Notably, $\mathrm{CER_{Ret}}$ with uncertainty of 8.36 μm shows closer agreement with $\mathrm{CER_{RVOD}}$ at all heights within the cloud, suggesting that the CER retrieved using our method not only aligns with $\mathrm{CER_{MODIS}}$ at the cloud top but also exhibits a consistent vertical distribution, reinforcing the accuracy and robustness of our method across different cloud heights.

Fig. 7 shows the comparison of the COT retrieved by our method (hereafter $\mathrm{COT_{Ret}}$) with the COT product provided by MODIS (hereafter $\mathrm{COT_{MODIS}}$). The comparison is presented through the bias frequency distribution and the cumulative probability function (cdf) of the fraction error (i.e., the percentage of the ratio between bias and true value) by treating $\mathrm{COT_{MODIS}}$ as the true value. For 166 010 profiles where both

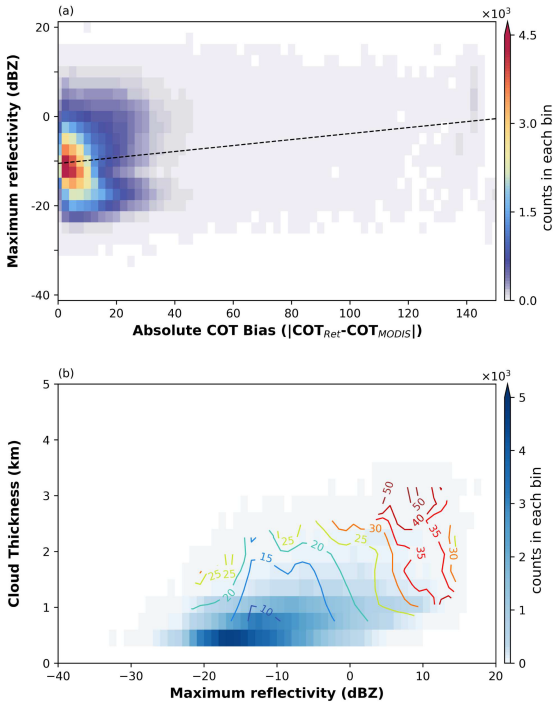

Fig. 8. Retrieved bias influenced by maximum reflectivity and cloud thickness. (a) Variation of absolute bias with maximum reflectivity. (b) Contour distribution of absolute bias with respect to maximum reflectivity and cloud thickness. The closer the color of the contour line is to a warmer color, the greater the value.

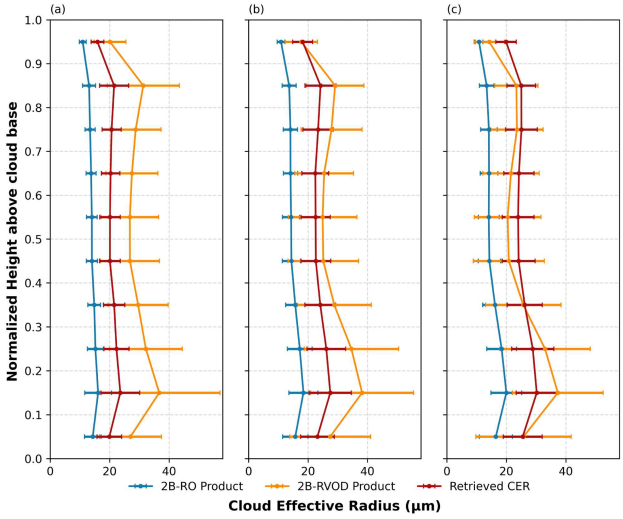

Fig. 9. Profiles of CER for (a) type 1, (b) type 2, and (c) type 3 versus the normalized height above cloud base (i.e., the ratio of each bin height from the cloud base to the cloud thickness) using the RO (blue), RVOD (orange) and the algorithm in this study (red). The mean and standard deviation of CER in each height bin are represented by a dot and a solid line, respectively.

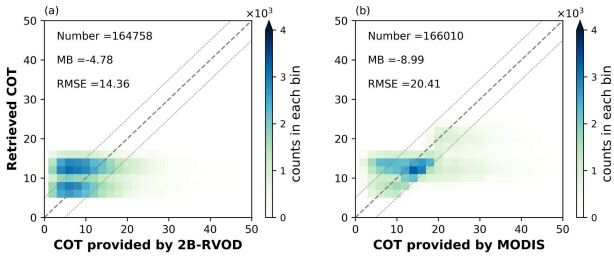

Fig. 10. Comparison of (a) COT retrieved by our method with the RVOD and (b) COT retrieved by using the CER at the cloud top with the MODIS product.

CloudSat and MODIS observations were available, $\mathrm{COT_{Ret}}$ is primarily concentrated below the diagonal, with the peak of the bias frequency shifted to the left of zero with uncertainty of 22.42, indicating that our retrieved COT is generally smaller than $\mathrm{COT_{MODIS}}$. The MB and RMSE between the two datasets are −11.33 and 22.42, respectively. This bias may be partly attributed to the difference in observational approach of the passive and active instruments, which sample different regions of the clouds. In addition to the error arising from the instrument itself, we also examine how the absolute bias varies with the maximum radar reflectivity across the entire cloud layer, as shown in Fig. 8(a). We found that the maximum reflectivity increases with the absolute bias, particularly when the reflectivity exceeds −15 dBZ, indicating that larger particles (associated with higher reflectivity) correspond to greater bias. To further investigate the cloud types contributing to this high deviation, we combined cloud geometric thickness and maximum reflectivity. As displayed in Fig. 8(b), the larger absolute biases (shown by red contours) are concentrated in the upper right corner of the blue shading plot, which corresponds to clouds with greater thickness and larger particles. This suggests that the COT retrieved by our method tends to be underestimated for thicker clouds with larger droplets, as compared with MODIS.

It is important to note that $\mathrm{COT_{MODIS}}$ is derived under the assumption that $\mathrm{CER^{\mathit{T}}_{MODIS}}$ varies linearly or remains constant throughout the cloud layer. However, this assumption may not hold true for thicker clouds with larger particles, leading to discrepancies between the assumed and actual vertical distribution of droplet sizes. To validate this hypothesis, we classified all profiles into three categories according to the bias between $\mathrm{COT_{Ret}}$ and $\mathrm{COT_{MODIS}}$: 1) bias>5 (hereafter type 1); 2) $-5 \leq$ bias ≤ 5 (hereafter type 2); and 3) bias < -5 (hereafter type 3). Then we compared the profiles of the $\mathrm{CER_{Ret}}$ with those of the CloudSat product in each category, as shown in the three columns of Fig. 9. Interestingly, for the third category (where the COT bias is less than −5), $\mathrm{CER_{Ret}}$ is closer to the $\mathrm{CER_{RVOD}}$ than in the other categories, suggesting that the smaller $\mathrm{COT_{Ret}}$ in this group can be attributed to differences in CER vertical distribution assumptions. Moreover, COT retrieved by our method shows high agreement with COT from the RVOD product [see Fig. 10(a)]. This confirms that the underestimation of COT retrieval is primarily due to the assumption of the CER vertical distribution in the MODIS product. Therefore, we further utilize only the $\mathrm{CER^{\mathit{T}}_{Ret}}$ and assume that the CER in the cloud layer varies with height, analogous to the MODIS retrieval algorithm, and obtain the COT according to the adiabatic theory as $\mathrm{COT^{\mathit{T}}_{Ret}} = (9\mathrm{LWP_{Ret}})/(5\mathrm{CER^{\mathit{T}}_{Ret}})$. In accordance with the results shown in Fig. 10(b), the recalculated $\mathrm{COT^{\mathit{T}}_{Ret}}$ are distributed near the diagonal with a smaller MB in comparison to and $\mathrm{COT_{MODIS}}$ (i.e., −8.99 versus −11.33). In other words, when $\mathrm{CER^{\mathit{T}}_{Ret}}$ is assumed to vary linearly with height, similar to the MODIS retrieval algorithm; the retrieved COT aligns

well with passive instrument products. It is firmly confirmed that the method proposed in this study, which includes a more detailed CER vertical structure, improves the accuracy of the COT retrieval, strengthening the importance of accounting for the full vertical distribution of cloud properties.

V. Conclusion and Discussion

In this study, we introduce innovative algorithms for retrieving cloud microphysical properties, specifically cloud LWC, CER, and COT from satellite-borne millimeter-wavelength CPR. These algorithms are grounded in radar detection principles and the intrinsic relationships between cloud properties, overcoming the constraints of traditional methods that rely on a priori data and synchronization across multiple instruments. Our approach leverages both the backscattering intensity and attenuation of radar waves, enabling more robust retrievals without dependence on passive instrument data, which often limit the accuracy and coverage of existing algorithms.

We assess the precision and efficacy of our method by applying it to data from the SO region, where low marine boundary layer clouds are prevalent, and compare the results with existing cloud property products from CloudSat and other passive remote sensing instruments. Our retrievals exhibit high accuracy, with cloud LWC, CER, and COT showing excellent agreement with independent reference products, such as the RVOD, AMSR2, and MODIS. The longitudinal, latitudinal, and vertical distributions of cloud LWC obtained by our method align closely with those from the RVOD product, demonstrating its ability to capture spatial patterns accurately. In addition, the retrieved cloud LWP is in close agreement with AMSR2, highlighting the potential of our method to deliver continuous cloud products throughout the day and night, which passive remote sensing instruments cannot achieve due to their limitations.

A key advantage of our method is its ability to retrieve CER with a high degree of accuracy. Not only do the retrieved CER values closely mirror the MODIS product at the cloud top, but they also exhibit a vertical distribution more consistent with the RVOD product compared with the RO product. This indicates that our approach captures the variability of cloud microphysical properties more effectively throughout the entire cloud layer. However, it is worth noting that the COT values retrieved by our method tend to be lower than those from MODIS. Through statistical analysis and comparison of the vertical distribution of CER within various COT bias categories, we identify that this underestimation is primarily due to the vertical structure of the CER retrieved by our method, which deviates from the assumptions made in the MODIS retrieval algorithm. This finding underscores the novelty of our algorithm, which provides more physically grounded vertical structures of cloud microphysical properties, leading to more accurate cloud property retrievals.

This study makes a significant advancement in cloud retrieval algorithms by overcoming the inherent limitations of existing methods, which often rely heavily on passive instruments or empirical data. By applying a top-down detection performance model to satellite remote sensing, our approach integrates both ground- and space-based radar measurements, offering a comprehensive and physically consistent framework for retrieving cloud properties. This algorithm marks a major step forward in cloud remote sensing by reducing dependence on passive instruments and preassumed cloud models, thereby improving the reliability of cloud property retrievals. Not only does this enhance the accuracy of cloud microphysical retrievals, but it also lays the foundation for more reliable cloud property representations in climate models. The continued application of this method to the 18 years of CloudSat data, as well as current spaceborne radar missions such as EarthCARE, holds the potential to significantly improve global cloud datasets. This could better capture the complex vertical structures of cloud properties and provide a more physically consistent representation of clouds in future climate simulations.

Appendix

According to (1), the relationship between the unattenuated and measured reflectivity can be rewritten as

$$aZ_e^b(h_i) = aZ_m^b(h_i)\, e^{0.46b\int_{h_t}^{h_i} k_c(s)ds}. \tag{A1}$$

Considering that $k_c = K^*\mathrm{LWC}$ and $\mathrm{LWC} = aZ_e^b = b$, (A1) can be transformed into

$$aZ_e^b(h_i) = aZ_m^b(h_i)\, e^{0.46bK^*\int_{h_t}^{h_i} aZ_e^b(s)ds}. \tag{A2}$$

Assuming that

$$x = 0.46K^*\int_{r_0}^{r_i} aZ_e^b(s)\,ds \tag{A3}$$

and

$$v = e^{bx}. \tag{A4}$$

Based on (A3)–(A4), the following differential equations can be obtained:

$$\begin{aligned} dx &= 0.46K^* aZ_e^b(r)\,dr \\ dv &= bv dx. \end{aligned} \tag{A5}$$

Thus the Z_e can be expressed as

$$aZ_e^b(r) = \frac{1}{0.46K^*}\frac{dx}{dr} = \frac{1}{0.46K^*}\frac{dv}{bvdr}. \tag{A6}$$

By combining (A2) and (A6), we can obtain the formulas as

$$\frac{1}{0.46K^*}\frac{dv}{bvdr} = aZ_m^b v. \tag{A7}$$

Namely, from the (A7), the Bernoulli differential equation is established as

$$\begin{aligned} \frac{dv}{v^2} &= 0.46abK^* Z_m^b dr \\ v &= e^{bx} \\ x &= 0.46K^*\int_{r_0}^{r} aZ_e^b(s)\,ds. \end{aligned} \tag{A8}$$

By integrating (A8) from h_t to h_i and h_l, respectively, the relationship between $\mathrm{LWC}(h_i)$, $Z_m(h_i)$ and $\mathrm{LWC}(h_l)$ can be established as

$$\mathrm{LWC}(h_i) = \frac{Z_m^b(h_i)\,\mathrm{LWC}(h_l)}{Z_m^b(h_l) + \mathrm{LWC}(h_l)\, I(h_i, h_l)}$$

$$I(h_i, h_l) = \int_{h_i}^{h_l} 046bK^* Z_m^b(s)\, ds. \tag{A9}$$

Referring to the details of the retrieval method for ground-based radar [43], the LWC(h_l) can be further expressed as

$$\mathrm{LWC}(h_l) = \frac{Z_m^b(h_l)}{I(h_t, h_l)} \left[\exp(0.46bK^* \mathrm{LWP}) - 1\right]. \tag{A10}$$

By substituting (A10) into (A9), one can see that the LWC at any range between h_t and h_l [i.e., LWC(h_i)] can be expressed in (2).

ACKNOWLEDGMENT

The authors would like to thank the National Aeronautics and Space Administration (NASA) for supporting the satellite data (i.e., CloudSat, MODIS, and AMSR2) used in this study (https://www.earthdata.nasa.gov/).

REFERENCES

[1] T. L. Kubar, D. L. Hartmann, and R. Wood, "Understanding the importance of microphysics and macrophysics for warm rain in marine low clouds. Part I: Satellite observations," *J. Atmos. Sci.*, vol. 66, no. 10, pp. 2953–2972, Oct. 2009, doi: 10.1175/2009jas3071.1.

[2] R. D. Cess et al., "Cloud feedback in atmospheric general circulation models: An update," *J. Geophys. Res.*, vol. 101, no. D8, pp. 12791–12794, May 1996, doi: 10.1029/96jd00822.

[3] R. T. Wetherald and S. Manabe, "Cloud feedback processes in a general circulation model," *J. Atmos. Sci.*, vol. 45, no. 8, pp. 1397–1416, Apr. 1988.

[4] M. Wild, D. Folini, C. Schär, N. Loeb, E. G. Dutton, and G. König-Langlo, "The global energy balance from a surface perspective," *Climate Dyn.*, vol. 40, nos. 11–12, pp. 3107–3134, Jun. 2013, doi: 10.1007/s00382-012-1569-8.

[5] S. L. Fiddes, A. Protat, M. D. Mallet, S. P. Alexander, and M. T. Woodhouse, "Southern Ocean cloud and shortwave radiation biases in a nudged climate model simulation: Does the model ever get it right?," *Atmos. Chem. Phys.*, vol. 22, no. 22, pp. 14603–14630, Nov. 2022, doi: 10.5194/acp-22-14603-2022.

[6] E. Tansey, R. Marchand, S. P. Alexander, A. R. Klekociuk, and A. Protat, "Southern Ocean low cloud and precipitation phase observed during the Macquarie Island cloud and radiation experiment (MICRE)," *J. Geophys. Res., Atmos.*, vol. 128, no. 17, Sep. 2023, Art. no. 17, doi: 10.1029/2023jd039205.

[7] H. Tietäväinen and T. Vihma, "Atmospheric moisture budget over Antarctica and the Southern Ocean based on the ERA-40 reanalysis," *Int. J. Climatol.*, vol. 28, no. 15, pp. 1977–1995, Dec. 2008, doi: 10.1002/joc.1684.

[8] K. E. Trenberth and J. T. Fasullo, "Simulation of present-day and twenty-first-century energy budgets of the Southern Oceans," *J. Climate*, vol. 23, no. 2, pp. 440–454, Jan. 2010, doi: 10.1175/2009jcli3152.1.

[9] Y.-T. Hwang and D. M. W. Frierson, "Link between the double-intertropical convergence zone problem and cloud biases over the Southern Ocean," *Proc. Nat. Acad. Sci. USA*, vol. 110, no. 13, pp. 4935–4940, Mar. 2013, doi: 10.1073/pnas.1213302110.

[10] J. Li et al., "Retrieval of cloud microphysical properties from MODIS and AIRS," *J. Appl. Meteorol.*, vol. 44, no. 10, pp. 1526–1543, Oct. 2005, doi: 10.1175/jam2281.1.

[11] K. Ohara, T. Kubota, M. Kachi, and M. Kazumori, "Comparison of long-term total precipitable water products by the advanced microwave scanning radiometer 2 (AMSR2)," *J. Meteorological Soc. Japan. Ser. II*, vol. 101, no. 4, 2023, Art. no. 4, doi: 10.2151/jmsj.2023-018.

[12] S. Platnick et al., "The MODIS cloud optical and microphysical products: Collection 6 updates and examples from Terra and Aqua," *IEEE Trans. Geosci. Remote Sens.*, vol. 55, no. 1, pp. 502–525, Jan. 2017, doi: 10.1109/TGRS.2016.2610522.

[13] M. Min, P. Wang, J. R. Campbell, X. Zong, and J. Xia, "Cirrus cloud macrophysical and optical properties over north China from CALIOP measurements," *Adv. Atmos. Sci.*, vol. 28, no. 3, pp. 653–664, May 2011, doi: 10.1007/s00376-010-0049-5.

[14] H. Okamoto et al., "Cloud masks and cloud type classification using EarthCARE CPR and ATLID," *Atmos. Meas. Techn. Discuss.*, vol. 2024, pp. 1–21, Jul. 2024.

[15] N. Tomiyama et al., "EarthCARE/CPR development status and performance," *Proc. SPIE*, vol. 11531, pp. 109–116, Aug. 2020, doi: 10.1117/12.2574244.

[16] L. Zang et al., "CALIOP retrieval of droplet effective radius accounting for cloud vertical homogeneity," *Opt. Exp.*, vol. 29, no. 14, p. 21921, 2021, doi: 10.1364/oe.427022.

[17] J. Wang, C. Liu, M. Min, X. Hu, Q. Lu, and L. Husi, "Effects and applications of satellite radiometer 2.25-μ m channel on cloud property retrievals," *IEEE Trans. Geosci. Remote Sens.*, vol. 56, no. 9, pp. 5207–5216, Sep. 2018, doi: 10.1109/TGRS.2018.2812082.

[18] H. Yeo et al., "Arctic cloud properties and associated radiative effects in the three newer reanalysis datasets (ERA5, MERRA-2, JRA-55): Discrepancies and possible causes," *Atmos. Res.*, vol. 270, Jun. 2022, Art. no. 106080, doi: 10.1016/j.atmosres.2022.106080.

[19] S. P. Alexander and A. Protat, "Cloud properties observed from the surface and by satellite at the northern edge of the Southern Ocean," *J. Geophys. Res., Atmos.*, vol. 123, no. 1, pp. 443–456, Jan. 2018, doi: 10.1002/2017jd026552.

[20] E. E. Clothiaux et al., "An evaluation of a 94-GHz radar for remote sensing of cloud properties," *J. Atmos. Ocean. Technol.*, vol. 12, no. 2, pp. 201–229, Apr. 1995.

[21] L. Kou, Z. Lin, H. Gao, S. Liao, and P. Ding, "Simulation and sensitivity analysis for cloud and precipitation measurements via space-borne millimeter-wave radar," *Atmos. Meas. Techn.*, vol. 16, no. 6, pp. 1723–1744, Mar. 2023, doi: 10.5194/amt-16-1723-2023.

[22] X. Hu, J. Ge, Y. Li, R. Marchand, J. Huang, and Q. Fu, "Improved hydrometeor detection method: An application to CloudSat," *Earth Space Sci.*, vol. 7, no. 2, p. 2019, Feb. 2020, doi: 10.1029/2019ea000900.

[23] S. Tanelli et al., "CloudSat's cloud profiling radar after two years in orbit: Performance, calibration, and processing," *IEEE Trans. Geosci. Remote Sens.*, vol. 46, no. 11, pp. 3560–3573, Nov. 2008, doi: 10.1109/TGRS.2008.2002030.

[24] R. T. Austin. (2007). *Level 2B Radar-Only Cloud Water Content (2B-CWC-RO) Process Description Document*. Data Process. Center. Accessed: May 14, 2024. [Online]. Available: https://www.cloudsat.cira.colostate.edu/cloudsat-static/info/dl/2b-cwc-ro/2B-CWC-RO_PDICD.P_R04.20071021.pdf

[25] R. T. Austin and G. L. Stephens, "Retrieval of stratus cloud microphysical parameters using millimeter-wave radar and visible optical depth in preparation for CloudSat: 1. algorithm formulation," *J. Geophys. Res. Atmos.*, vol. 106, no. D22, pp. 28233–28242, Nov. 2001, doi: 10.1029/2000jd000293.

[26] N. Wood, "Level 2B radar-visible optical depth cloud water content (2B-CWC-RVOD) process description document," *Version*, vol. 5, pp. 1–26, Jun. 2008.

[27] G. de Boer, G. J. Tripoli, and E. W. Eloranta, "Preliminary comparison of CloudSAT-derived microphysical quantities with ground-based measurements for mixed-phase cloud research in the Arctic," *J. Geophys. Res. Atmos.*, vol. 113, no. D8, Apr. 2008, Art. no. D8, doi: 10.1029/2008jd010029.

[28] M. Lebsock and H. Su, "Application of active spaceborne remote sensing for understanding biases between passive cloud water path retrievals," *J. Geophys. Res., Atmos.*, vol. 119, no. 14, pp. 8962–8979, Jul. 2014, doi: 10.1002/2014jd021568.

[29] Y.-J. Noh, C. J. Seaman, T. H. Vonder Haar, D. R. Hudak, and P. Rodriguez, "Comparisons and analyses of aircraft and satellite observations for wintertime mixed-phase clouds," *J. Geophys. Res.*, vol. 116, no. D18, Sep. 2011, Art. no. D18, doi: 10.1029/2010jd015420.

[30] C. Zhao et al., "Toward understanding of differences in current cloud retrievals of ARM ground-based measurements," *J. Geophys. Res., Atmos.*, vol. 117, May 2012, Art. no. D10, doi: 10.1029/2011jd016792.

[31] B. Pan et al., "Intercomparisons on the vertical profiles of cloud microphysical properties from CloudSat retrievals over the north China plain," *J. Geophys. Res., Atmos.*, vol. 128, no. 13, Jul. 2023, Art. no. 13, doi: 10.1029/2023jd039093.

[32] R. M. Schulte, M. D. Lebsock, and J. M. Haynes, "What CloudSat cannot see: Liquid water content profiles inferred from MODIS and CALIOP observations," *Atmos. Meas. Techn.*, vol. 16, no. 14, pp. 3531–3546, Jul. 2023, doi: 10.5194/amt-16-3531-2023.

[33] A. Gettelman et al., "Simulating observations of Southern Ocean clouds and implications for climate," *J. Geophys. Res., Atmos.*, vol. 125, no. 21, Nov. 2020, Art. no. 21, doi: 10.1029/2020jd032619.

[34] Y. Huang, S. T. Siems, M. J. Manton, A. Protat, and J. Delanoë, "A study on the low-altitude clouds over the Southern Ocean using the DARDAR-MASK," *J. Geophys. Res., Atmos.*, vol. 117, no. D18, Sep. 2012, Art. no. D18, doi: 10.1029/2012jd017800.

[35] G. Lin, S. Sillman, J. E. Penner, and A. Ito, "Global modeling of SOA: The use of different mechanisms for aqueous-phase formation," *Atmos. Chem. Phys.*, vol. 14, no. 11, pp. 5451–5475, Jun. 2014, doi: 10.5194/acp-14-5451-2014.
[36] D. T. McCoy et al., "Natural aerosols explain seasonal and spatial patterns of Southern Ocean cloud albedo," *Sci. Adv.*, vol. 1, no. 6, Jul. 2015, Art. no. 6, doi: 10.1126/sciadv.1500157.
[37] K. Sassen, Z. Wang, and D. Liu, "Global distribution of cirrus clouds from cloudsat/cloud-aerosol LiDAR and infrared pathfinder satellite observations (CALIPSO) measurements," *J. Geophys. Res., Atmos.*, vol. 113, no. D8, Apr. 2008, Art. no. D8, doi: 10.1029/2008jd009972.
[38] C. L. Gentemann and K. A. Hilburn, "In situ validation of sea surface temperatures from the GCOM-W1 AMSR2 RSS calibrated brightness temperatures," *J. Geophys. Res., Oceans*, vol. 120, no. 5, pp. 3567–3585, May 2015, doi: 10.1002/2014jc010574.
[39] P. Minnis et al., "CERES MODIS cloud product retrievals for edition 4—Part I: Algorithm changes," *IEEE Trans. Geosci. Remote Sens.*, vol. 59, no. 4, pp. 2744–2780, Apr. 2021, doi: 10.1109/TGRS.2020.3008866.
[40] M. Kazumori, "Precipitable water vapor retrieval over land from GCOM-W/AMSR2 and its application to numerical weather prediction," in *Proc. IEEE Int. Geosci. Remote Sens. Symp. (IGARSS)*, Jul. 2018, pp. 6663–6666, doi: 10.1109/IGARSS.2018.8517771.
[41] S. Platnick et al., "The MODIS cloud products: Algorithms and examples from Terra," *IEEE Trans. Geosci. Remote Sens.*, vol. 41, no. 2, pp. 459–473, Feb. 2003, doi: 10.1109/TGRS.2002.808301.
[42] D. Painemal, T. Greenwald, M. Cadeddu, and P. Minnis, "First extended validation of satellite microwave liquid water path with ship-based observations of marine low clouds," *Geophys. Res. Lett.*, vol. 43, no. 12, pp. 6563–6570, Jun. 2016, doi: 10.1002/2016gl069061.
[43] J. Ge et al., "A novel liquid water content retrieval method based on mass absorption for single-wavelength cloud radar," *IEEE Trans. Geosci. Remote Sens.*, vol. 61, 2023, Art. no. 4102815, doi: 10.1109/TGRS.2023.3278735.
[44] J. Du et al., "An accurate retrieval of cloud droplet effective radius for single-wavelength cloud radar," *IEEE Trans. Geosci. Remote Sens.*, vol. 62, 2024, Art. no. 4108511, doi: 10.1109/TGRS.2024.3447002.
[45] P. K. Wang, "Theoretical studies on the motions of cloud and precipitation particles—A review," *Meteorology*, vol. 1, no. 3, pp. 288–310, Aug. 2022, doi: 10.3390/meteorology1030019.

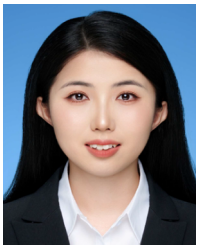

Jiajing Du received the B.S. and Ph.D. degrees in atmospheric science from Lanzhou University, Lanzhou, China, in 2019 and 2025, respectively.

She is an Assistant Researcher with the Heavy Rain and Drought-Flood Disasters in Plateau and Basin Key Laboratory of Sichuan Province, Institute of Plateau Meteorology, China Meteorological Administration, Chengdu, China. Her research interests include radar data processing and cloud physical properties retrieval algorithms.

Jinming Ge received the B.S. and Ph.D. degrees in atmospheric science from Lanzhou University, Lanzhou, China, in 2005 and 2010, respectively.

From 2010 to 2012, he was a Lecturer with Lanzhou University, where he became an Associate Professor in 2012, and has been a Professor since 2017. He is currently a Professor with the Key Laboratory for Semi-Arid Climate Change of the Ministry of Education and College of Atmospheric Sciences, Lanzhou University. His research interests include atmospheric aerosols, cloud physical properties retrieval, and their radiative effects on climate.

Jianping Huang received the Ph.D. degree in weather dynamics from Lanzhou University, Lanzhou, China, in 1988.

He performed post-doctoral work at Peking University, Beijing, China. He is an Academician of Chinese Academy of Sciences and a Professor of the Key Laboratory for Semi-Arid Climate Change of the Ministry of Education and College of Atmospheric Sciences, Lanzhou University. He is the main author of the first working group of the Working Group I of the Fifth Assessment Report of the IPCC, and is one of the academic leaders in the field of atmospheric science in China who has combined systematic observation and theoretical research and made major breakthroughs. He plays an important role in semi-arid climate research in China. He created and developed the first semi-arid climate comprehensive observation station with international standards in western China. His research interests include global arid and semi-arid regions and the interaction of dust aerosols with clouds and precipitation.

Yize Li, received the B.S. degree from Shenyang Agricultural University, Shenyang, China, in 2020. She is currently pursuing the Ph.D. degree with Lanzhou University, Lanzhou, China.

Her research interests include the relationship between clouds and the meteorological field, and the cloud radiation feedback effect.

Chi Zhang, received the B.S. degree in atmospheric science from Chengdu University of Information Technology, Chengdu, China, in 2021. He is currently pursuing the Ph.D. degree with Lanzhou University, Lanzhou, China.

His research interests include millimeter-wave radar data processing and its application in studying diurnal variations of clouds.

Xiaoyu Hu, received the Ph.D. degree in atmospheric physics and atmospheric environment from Lanzhou University, Lanzhou, China, in 2022.

He is currently an Associate Researcher at Chongqing Research Institute of Big Data, Chongqing, China. His research interests include remote sensing of clouds and artificial intelligence applications in remote sensing.

Bochun Liu, received the B.S. degree in atmospheric science from Lanzhou University, Lanzhou, China, in 2022, where he is currently pursuing the Ph.D. degree in atmospheric physics and atmospheric environment.

His research interests include cloud detection, convective cloud detection and tracking, and convective cloud characteristics research.

Xiaojie Li, received the B.S. degree in atmospheric science from Lanzhou University, Lanzhou, China, in 2023, where he is currently pursuing the M.S. degree.

His research interests include millimeter-wave radar data processing, the microphysical properties of clouds, and their retrieval.

Yucheng Qiu, received the B.S. degree in atmospheric science from Chengdu University of Information Technology, Chengdu, China, in 2023. He is currently pursuing the M.S. degree with Lanzhou University, Lanzhou, China.

His research interests include precipitation signal detection and spatiotemporal distribution of global precipitation.

Yuhang Zhu, is currently pursuing the B.S. degree with Lanzhou University, Lanzhou, China.

His research interests include precipitation signal processing and mechanism analysis using cloud radar satellite data.